ASM Handbook Volume 22 – Modeling and Simulation: Processing of Metallic Materials

9. Simulation of PM Processes

9.A. Press and Sinter Powder Metallurgy

Suk Hwan Chung[1], Young-Sam Kwon[2], Seong Jin Park[3], and Randall M. German[4]

[1] Hyundai Steel Co., 167-32, Kodae-Ri, Songak-Myeon, Dangjin-Gun, Chungnam, 343-711 Korea
[2] CetaTech, Inc., TIC 296-3, Seonjin-Ri, Sacheon-Si, Kyongnam, 664-953 Korea
[3] Center for Advanced Vehicular Systems, Mississippi State University, 200 Research Blvd., Starkville, MS 39759, USA
[4] College of Engineering, San Diego State University, 5500 Campanile Drive, San Diego, CA 92182-1326

Introduction

Effective computer simulations of metal powder compaction and sintering are at the top of the powder metallurgy industry's wish list. There is much anticipated advantage to such efforts, yet there are problems that will inhibit widespread implementation. Press-sinter powder metallurgy computer simulations currently focus on the use of minimal input data to help with process set-up. Although the simulations are reasonably accurate, a large data array is required to hone in on current industrial practice. For example, final dimensions for automotive transmission gears are required to be held within 10 μm, but the simulations are not capable of such accuracy. Simple factors such as frictional tool heating are missing from the simulations. Additionally, powders vary in particle size distribution between production lots, but the simulations assume a nominally uniform powder. Since it is expensive to test each powder lot, the logic is to assume a nominal set of characteristics. In production, such process and powder variations are handled by constant adaptive control techniques. As an example, when an outside door is opened on press room it is common that press adjustments will be required to hold sintered dimensions. The press-sinter powder metallurgy simulations have not advanced to such levels of sophistication. Instead, the press-sinter powder metallurgy simulations are used to help set-up production operations with heavy reliance on experienced operators to make final trial and error adjustments.

In practice, the variations in powder, press, tooling, and other process variables are handled using skilled technicians, quality charts, and adaptive process control that relies on frequent sampling and periodic equipment adjustments. The gap between press-sinter practice and modeling might close if more rapid data generation routes were developed. For example, a study on modeling the press-sinter production of a main bearing cap required 10,000 measures to isolate the behavior. It is not economically feasible to repeat this testing for each 20 ton lot of powder. Even so, a great benefit comes from the fact that the computer simulations have forced the technical community to organize our knowledge and determine where there are problems.

Computer simulations of press-sinter operations trace to the 1960s [1-20]. The early simulations were generally unstable and two-dimensional (for example the sintering of aligned wires). By 1975, a variety of two-dimensional sintering approaches existed. With the expansion in computer power, the implementation of three-dimensional simulations arose to provide realistic outputs. In more recent times, the simulations have provided valuable three-dimensional treatments to predict the final component size and shape after sintering. Since the pressed green body is not homogeneous, backward solutions are desired to select the powder, compaction, and sintering attributes required to deliver the target properties with different tool designs, compaction presses, and sintering furnaces. In building toward this goal, various simulation types have been evaluated: Monte Carlo, Finite Difference, Discrete Element, Finite Element, Fluid Mechanics, Continuum Mechanics, Neural Network, and Adaptive Learning. Unfortunately, the input data and some of the basic relations are not well developed; accurate data are missing for most materials under the relevant conditions. For example, rarely is the strength measured for a steel alloy at the typical 1120°C sintering temperature. Further, constitutive models do not exist for the conditions relevant to sintering; for example, friction in die compaction changes during the split-second pressure stroke since lubricant (polymer) particles deform and undergo viscous flow to the die wall, effectively changing friction constantly during compaction. Thus, the simulations are approximations using extrapolated data and simplified relations. For this reason, computer simulations of press-sinter routes work best in the set-up mode. The simulations help define the processing window and set initial operating parameters. Presented here is information relevant to computer simulation of first article production, what is best termed "set-up" calculations, realizing that practice relies heavily on adaptive process control to keep the product in specification after the initial set-up is accomplished.

Brief History

The first major publication on computer simulation of sintering came out in 1965 [1]. Early simulations were two-dimensional (sintering two wires) with a single diffusion mechanism. These simulations were slow, requiring ten times more computer time than the actual physical sintering time. Most damaging, these early models were unstable since they lost volume and increased energy. However, within 20 years the concept was extended to include multiple transport mechanisms, multiple sintering stages, and even pressure-assisted sintering [6,9-11]. These simulations predicted density versus compaction pressure, sintering time, peak temperature, heating rate, green density, and particle size.

One of the first realizations was the limitations arising from the assumed isothermal conditions and simplistic microstructure coarsening. Dilatometry experiments show most sintering occurs on the way to the peak temperature, so isothermal models poorly reflect actual behavior [20]. Indeed, production powder metallurgy often simply "kisses" the peak temperature, a situation far from what is assumed in the simulations. And the assumed homogeneous and ideal microstructure unrealistically limits the models. Today the sintering body first treated with a compaction or shaping simulation to predict the green microstructure gradients, and subsequent sintering simulations use those density gradients, via finite element analysis, to predict the final size, shape, and properties [16-19].

Theoretical Background and Governing Equations

The methodologies used to model the press and sinter powder metallurgy include continuum, micromechanical, multi-particle, and molecular dynamics approaches. These differ in length scales. Among the methodologies, continuum models have the benefit of shortest computing time, with an ability to predict relevant attributes such as the component density, grain size, and shape.

Mass, volume, and momentum conservation are evoked in the continuum approach. Although, such assumptions might seem obvious, still powder metallurgy processes are ill-behaved and difficult to properly simulate. For example, polymer are added to the powder for tool lubrication, but the polymers are pyrolyzed during sintering, resulting in 0.5 to 1.5 wt. % mass loss. Likewise, pore space is not conserved during compaction and sintering, so bulk volume is not conserved. Even so, mass conservation equations are invoked to track densification, while momentum conservation is used to follow force equilibrium, including the distortion effect from gravity. Energy conservation is also essential in the continuum approach. However, it is typical to assume temperature is uniform in the compact; set to room temperature during compaction and following an idealized thermal cycle (often isothermal) during sintering. Both are incorrect, since tool heating occurs with repeated compaction

strokes and compact position in the sintering furnace gives a lagging thermal history that depends on location. Indeed, since dimensional precision is the key to powder metallurgy, statistical audits have repeatedly found that subtle factors such as position in the furnace are root causes of dimensional scatter. For example, fluid flow and heat transport calculations show considerable temperature differences associated with atmosphere flow and component shadowing within a furnace. Since such details are not embraced by the models, the typical assumption is to ignore temperature distribution within the component, yet such factors are known to cause part distortion during production.

Additionally, constitutive relations are required to describe the response of the compact to mechanical force during compaction and sintering. Many powder metallurgy materials are formed by mixing powders that melt, react, diffuse, and alloy during sintering. This requires sophistication in the models to add phase transformations, alloying, and other factors, many of which depend on particle size and other variations [15]. From conservation laws and constitutive relations, a system of partial differential equations is created that includes the initial and boundary conditions. These need to be integrated with microstructure and property models so that final compact properties can be predicted. Since the constitutive relations for compaction and sintering are completely different, they are described here in two separate sections.

Constitutive Relation during Compaction

Continuum plasticity models are frequently used to describe the mechanical response of metal powders during compaction. These phenomenological models, originally developed in soil mechanics, are characterized by a yield criterion, a hardening function, and a flow rule. Representative models include those known as the Cam-Clay [21], Drucker-Prager-cap [22], and Shima-Oyane [23] models. Of these, the most successful for metal powders has been the Shima-Oyane model, although for ceramics, soils, and minerals other relations are generally more successful.

The typical initial and boundary conditions during compaction are as follows:
- Initial condition for the powder: tap density
- Boundary conditions: velocity prescribed in upper and bottom punches and friction condition in the tooling side wall; usually assumed the same for all tool surfaces independent of wear and independent of lubricant flow during the compaction stroke.

During compaction and ejection, a damage model, such as the Drucker-Prager failure surface [22] and failure separation length (FSL) idea [111] is required. To predict crack formation,

the FSL assumes there is an accumulated separation length from the Drucker-Prager failure surface, which provides the possibility of crack formation, as shown in Figure 1. The equation for the FSL is expressed as follows:

$$F_S = q + p \tan \beta - d .$$ (1)

where q and p are the effective stress and hydrostatic pressure. Note that d and β are the offset stress and slope for Drucker-Prager failure surface shown in Figure 1. Since the models predict green density versus location, then defect sensitivity is possible. For example, elastic relaxation occurs on ejection and if the stress exceeds the green strength, then green cracking occurs. It is in this area the compaction models are most effective.

Constitutive Relation during Sintering

Continuum modeling is the most relevant approach to modeling grain growth, densification, and deformation during sintering. Key contributions were by Ashby [6,9], McMeeking and Kuhn [25], Olevsky *et al.* [17,19], Riedel *et al.* [13,26,27], Bouvard and Meister [28], Cocks [29], Kwon *et al.* [30,31], and Bordia and Scherer [32-34] based on sintering mechanism such as surface diffusion, grain boundary diffusion, volume diffusion, viscous flow (for amorphous materials), plastic flow (for crystalline materials), evaporation-condensation, and rearrangement. For industrial application, the phenomenological models are used for sintering simulations with following key physical parameters:

- Sintering stress [20] is a driving force of sintering due to interfacial energy of pores and grain boundaries. Sintering stress depends on the material's surface energy, density, and geometric parameters such as grain size when all pores are closed in the final stage.
- Effective bulk viscosity is a resistance to densification during sintering and is a function of the material, porosity, grain size, and temperature. The model of the effective bulk viscosity has various forms according to the assumed dominant sintering mechanism.
- Effective shear viscosity is a resistance to deformation during sintering and is also a function of the material, porosity, grain size, and temperature. Several rheological models for the effective bulk viscosity are available.

The above parameters are function of grain size. Therefore, a grain growth model is needed for accurate prediction of densification and deformation during sintering.

Typical initial and boundary conditions for the sintering simulations include the following:

- Initial condition: mean particle size and grain size of the green compact for grain growth and initial green density distribution for densification obtained from compaction simulations.
- Boundary conditions: surface energy condition imposed on the free surface and friction condition of the component depending it is size, shape, and contact with the support substrate.

The initial green density distribution within the pressed body raises the necessity to start the sintering simulation with the output from an accurate compaction simulation, since die compaction induces green density gradients that depend on the material, pressure, rate of pressurization, tool motions, and lubrication. The initial and boundary conditions help determine the shape distortion during sintering from gravity, nonuniform heating, and from the green body density gradients.

Numerical Simulation

Even though many numerical methods have been developed, the finite element method (FEM) is most popular for continuum models of the press and sinter process. The FEM approach is a numerical computational method for solving a system of differential equations through approximation functions applied to each element, called domain-wise approximation. This method is very powerful for the typical complex geometries encountered in powder metallurgy. This is one of the earliest techniques applied to materials modeling, and is used throughout industry today. Many powerful commercial software packages are available for calculating two-dimensional (2D) and three- dimensional (3D) thermo-mechanical processes such as found in press and sinter powder metallurgy.

To increase the accuracy and convergence speed for the press and sinter simulations, developers of the simulation tools have selected explicit and implicit algorithms for time advancement, as well as numerical contact algorithms for problems such as surface separation, and remeshing algorithms as required for large deformations such as seen in some sintered materials, where up to 25 % dimensional contraction is possible.

Figure 2 shows the typical procedure for computer simulation for the press-sinter process, which consists of five components; simulation tool, pre- and post processors, optimization algorithm, and experimental capability. Pre- and post- processors are important to use the simulation tools efficiently. Pre-processor is a software tool to prepare input data for the simulation tool including computational domain preparation such as geometry modeling and mesh generator. Figure 3 is an example of the component, compaction, and sintering models, in this case for an oxygen sensor housing. To execute this model requires considerable input,

including material property database (including strain effects during compaction and temperature effects during sintering) and processing condition database (loading schedule of punches and dies for compaction simulation and heating cycle for sintering simulation). Post-processor is a software tool to visualize and analyze the simulation results, which enhances the usefulness of the simulations. From the standpoint of process set-up calculations, the optimization algorithm is essential to maximize computer simulation capability providing optimum part, die, and process condition design. Experimental capability is very important in computer simulation providing a means to evaluate changes in materials, powders, compaction schedules, heating cycles, and generally to provide verification of the simulation results.

Experimental Determination of Material Properties and Simulation Verification

Material Properties and Verification for Compaction

One of the first needs is to measure the powder density as a function of applied pressure to generate the material parameters in the constitutive model for compaction, including the Coulomb friction coefficient between the powder and die. Note these factors vary with the powder lot, lubricant, tool material, and even tool temperature. The procedure to obtain the material properties based on the generalized Shima-Oyane model is as follows [24]:

- Measure the pycnometer and tap densities of the powder.
- Conduct a series of uniaxial compression tests with die wall lubrication to minimize the die wall friction effect. The tap density is considered the starting point (after particle rearrangement) corresponding to zero compaction pressure. By curve fitting, six material parameters (α, γ, m, a, b, and n) are determined for the yield surface Φ as follows

$$\Phi = \left(\frac{q}{\sigma_m}\right)^2 + \alpha(1-D)^\gamma \left(\frac{p}{\sigma_m}\right) - D^m . \tag{2}$$

  where q and p are the effective stress and hydrostatic stress or pressure, D is the relative or fractional density, and σ_m is the flow stress of matrix material which is expressed as

$$\sigma_m = a + b\bar{\varepsilon}_m^n . \tag{3}$$

  where $\bar{\varepsilon}_m$ is the effective strain of matrix material.

- Series of uniaxial compression tests are performed *without* wall lubricant then the Coulomb frictional coefficient is obtained by FEM simulation.

7

Figure 4 is an illustration of the compaction curve for an iron-based powder (Distaloy AE, Höganäs) in a simple cylindrical geometry. Uniaxial compression tests are provided for two samples, the smaller sample of 2 g in a 12 mm diameter die with die wall lubrication and the larger sample of 8 g without wall lubrication. By curve fitting, the six material parameters are as follows [24]:

$$\alpha = 6.20,\ \gamma = 1.03,\ m = 7.40,\ a = 184\ \text{MPa},\ b = 200\ \text{MPa, and}\ n = 0.240.$$

By FEM simulation, the Coulomb frictional coefficient was obtained as 0.1. Table 1 shows the example of complete set of material properties of iron-based powder as input data for the compaction simulation.

Verification of the predicted density gradients in the green compact has been approached by many techniques. The most reliable, direct, and most sensitive comes from taking hardness or microhardness traces on a polished cross-section. Thus, to verify the compaction simulation results, the relation between hardness and green density is conducted according to the following procedure:

- Use the same samples as used for obtaining the material parameters
- Pre-sinter the compacts at a temperature sufficient to bond the particles but below the temperature range where dimensional change or chemical reactions occurs.
- Carefully prepare a metallographic cross-section of the pre-sintered samples and treat with a vacuum annealing cycle to minimize any hardness change induced by the cutting process.
- Measure hardness of each sample with a known green density and from that develop a correlation between density and hardness.
- Apply the same procedure and hardness traces to real components and from precise measures of hardness and location develop contour plot of the green density distribution for comparison with the computer simulation.

As an example, Figure 5 is a plot of the correlation between green density and hardness for WC-Co system. For this plot, pre-sintering cycle of WC-Co system was at 790$^\text{o}$C for 30 min, and the annealing cycle of was at 520$^\text{o}$C for 60 min, and in this case Rockwell 15T hardness scale was used. The obtained correlation is as follows [35]:

$$D = 0.638 + 1.67 \cdot 10^{-3} H - 5.44 \cdot 10^{-7} H^2. \tag{4}$$

where H is the 15T Rockwell hardness number and D is the fractional density. Figure 6

compares the simulation results taken using a commercial software package (PMsolver) with the experiment results for a cutting tool geometry formed from a cemented carbide powder based on Equation (4).

Material Properties and Verification for Sintering

In the development of a constitutive model for the sintering simulation, a wide variety of tests are required, including data on grain growth, densification (or swelling), and distortion. These are approached as follows:

- Grain growth: Quenching tests are conducted from various points in the heating cycle and the mounted cross-sections are analyzed to obtain grain size data to implement grain growth models. A vertical quench furnace is used to sinter the compacts to various points in the sintering cycle and then to quench those compacts in water. This gives density, chemical dissolution (for example diffusion of one constituent into another), and grain size as instantaneous functions of temperature and time. The quenched samples are sectioned, mounted, and polished prior to optical or scanning electron microscopy (SEM). Today, automated quantitative image analysis provides rapid determination of density, grain size, and phase content versus location in the compact. Usually during sintering the mean grain size G varies from the starting mean grain size G_0 (determined on the green compact). A new master sintering curve concept is applied to fit the experimental grain size data to an integral work of sintering [36], since actual cycles are a complex combination of heats and holds. The resulting material parameters trace to an apparent activation energy as the only adjustable parameter. Figure 7 shows SEM micrographs after quenching test and grain growth modeling for a W – 8.4 wt.% Ni – 3.6 wt.% Fe mixed powder compact during liquid phase sintering.

- Densification: To obtain material parameters for densification, constant heating rate dilatometry is used for *in situ* measurement of shrinkage, shrinkage rate, and temperature. By fitting the experimental data to models that include the sintering stress σ_s and bulk viscosity K as functions of density and grain size, again relying on the master sintering curve concept [37], the few unknown material parameters are extracted. Figure 8 shows the dilatometry data and model curve-fitting results used to obtain the missing material parameters during sintering of a 316L stainless steel [38].

- Distortion: Powder metallurgy compacts reach very low strength levels during sintering. Accordingly, weak forces such as gravity, substrate friction, and nonuniform heating will induce distortion and even cracking. To obtain the material parameters related to distortion, three point bending or sinter forging experiments are used for *in situ* measurement of distortion [39]. By fitting the experimental data with FEM

simulations for shear viscosity μ with grain growth, the parameters such as apparent activation energy and reference shear viscosity are extracted. Figure 9 shows *In situ* bending test and FEM results for obtaining material parameters in shear viscosity for a 316L stainless steel powder doped with 0.2% boron to induce improved sintering.

Such data extraction techniques have been allied to several materials, ranging from tungsten alloys, molybdenum, zirconia, cemented carbides, niobium, steel, stainless steel, and alumina. Table 2 is an example set of material properties for W – 8.4 wt.% Ni – 3.6 wt.% Fe as used as input data for the sintering simulation [40]. The above experiment techniques can be used for verification of sintering simulation results.

Demonstration of System Use

Time Advance Algorithm and Compaction Simulation Accuracy

Time advance in the simulation models is a concern with respect to the balance between accuracy and computational speed. The explicit method is fast, but sometimes exhibits convergence and accuracy problems, while the implicit method is accurate but slow. Figure 10 illustrates this case for a simple cylindrical geometry in the WC-Co system [35]. As shown in Figure 10b, the implicit method is more accurate for this case.

Gravitational Distorting in Sintering

The rheological data for the sintering system allows the system to respond to the internal sintering stress that drives densification and any external stress, such as gravity, that drives distortion. When a compact is sintered to high density it is also necessary to induce a low strength (the material is thermally softened to a point where the internal sintering stress can induce densification). Figure 11 shows sintering simulation results for a tungsten heavy alloy, relying on test data taken on Earth and under microgravity conditions, to then predict the expected shapes for various gravitational conditions - Earth, Moon, Mars, and in space. The results show that gravity affects shape distortion during sintering [40]. Accordingly, the computer simulations can be used to reverse engineer the green component geometry to anticipate the distortion to achieve the desired sintered part design.

Compaction Optimization

There are two different simulation approaches used to optimize die compaction. One is based on the concept of "design of experiment" (DOE) and the other is a derivative based

optimization scheme. The process designer needs to first select a reasonable initial guess, objective function that needs to be minimized, and design variables for both approaches.

Figure 12 shows the first approach used to optimize the loading schedule to generate a uniform green density during die compaction [35]. In this case the target is a cutting tool formed from WC-Co. The displacement of upper punch was set as the design variable and the lower punch displacement was automatically calculated because the final dimension was fixed. The objective function was set to the standard deviation in green density, which is called the nonuniformity, and this was to be minimized. Figure 12a plots the density histograms for five different processing conditions. The first one (black) is the initial compaction process design and the fourth one (yellow) shows the optimum design for maximum uniformity with only a change in the upper punch motion. The density distributions of those two cases are shown in Figure 12b. For optimization in more complicated systems, the Taguchi method with orthogonal array can be used to create simulation experiments to efficiently isolate solutions.

In using a derivative based optimization scheme, it is important to define the searching direction and stepping size. The searching direction is decided by the direct differentiation method or adjoint variable method and the stepping size is usually selected by polynomial curve fitting. Using the results of finite element simulation with mesh system generated by the given design variables, design sensitivities are calculated by the algorithm of searching direction. The searching direction is selected by the conjugate gradient method and the proper stepping size is selected by the polynomial curve fitting, with the objective functions obtained by additional finite element simulations. The design parameters are iteratively updated until the convergence criteria are satisfied. Figure 13 shows the procedure of this approach to optimize loading schedule to have uniform density distribution during die compaction for hub part formed using a steel alloy powder [24]. The design variables considered in this example were the loading schedules of upper, inner lower, core rod, and die, and the objective function is the nonuniformity after die compaction. The goal was to minimize the nonuniformity. Figure 13a shows compaction tool set and analysis domain. Figure 13b plots the objective function during optimization and Figure 13c plots the density distributions of initial and optimum designs.

Sintering Optimization

Usually a small grain size is desired to improve properties for a given sinter density. In this illustration, the design variable is the sintering cycle. To obtain maximum density and minimum grain size, the following objective function F is proposed [41],

$$F = \alpha \left[\frac{\Delta\rho}{\rho} \right] + (1 - \alpha) \left[\frac{\Delta G}{G} \right]. \tag{5}$$

where α is an adjustable parameter. Figure 14 shows an example for maximum density and minimum grain size for a 17-4 PH stainless steel powder. For example, the minimum grain size will be 21.9 μm if the specified sintered density is 95 % or theoretical. Figure 14b shows the corresponding sintering cycle by matching the value of adjustable parameter α.

Coupled Press and Sinter Optimization

Coupled simulations are necessary to predict the quality of the final component after the combined press and sinter operations. Figure 15 illustrates this for the case for a shaped cutting tool formed from WC-Co. In practice, the final component exhibited cracking along the corners, but there was no sign of cracking after die compaction, as shown in Figure 15b. From the simulation results for initial design, the density distribution is found to vary from a fractional density of 0.583 to 0.814. After optimization of the tool loading schedule with the objection function to make the green density as uniform as possible, the green density distribution ranged from 0.638 to 0.675. Implementation of this loading cycle resulted in elimination of cracking in the sintered component.

Figure 16 is another illustration, in this case where the distortion in final shape is examined for oxygen sensor components. After optimization of the tool loading schedule and the sintering cycle, the final distortion from the target shape is significantly reduced for both the holder and sleeve.

Conclusion

Computer simulations of the press-sinter cycle in powder metallurgy have advanced considerably, and in combination with standard finite element techniques show a tremendous ability to guide process set-up. Illustrated here are the compaction and sintering concepts required to perform process optimization, typically via selection of appropriate compaction tool motion. Although the models are only approximations to reality, still they are of value in forcing a careful inspection of what is understood about the press-sinter process. In this regard, the greatest value of modeling is in the forced organization of process knowledge.

There remain several barriers to widespread implementation. The largest is that traditional powder metallurgy is largely dependent on adaptive process control since many of the

important factors responsible for dimensional or quality variations are not measured. The variations in particle size, composition, tool wear, furnace location, and other factors such as reactions between particles during heating, all impact the important dimensional control aspects of press-sinter powder metallurgy. Although nominal properties, such as strength, hardness, or fatigue life are dominated by the average component density. In that regard, especially with respect to the initial process set-up, the computer simulations are of great value. Still, important attributes such as dimensional tolerances and internal cracks or other defects are outside the cost-benefit capabilities of existing simulations. Further, the very large number of materials, processes, tool materials, sintering furnaces, and process cycles makes it difficult to generalize; significant data collection is required to reach the tipping point where the simulations are off-the-shelf. Thus, much more research and training is required to move the simulations into a mode where they are widely applied in practice. Even so, commercial software is available and shows great value in the initial process definition to set-up a new component.

References

1.   F. A. Nichols and W. W. Mullins, "Morphological Changes of a Surface of Revolution due to Capillarity-Induced Surface Diffusion," *Journal of Applied Physics*, 1965, vol. 36, pp. 1826-1835.

2.   F. A. Nichols, "Theory of Sintering of Wires by Surface Diffusion," *Acta Metallurgica*, 1968, vol. 16, pp. 103-113.

3.   K. E. Easterling and A. R. Tholen, "Computer-Simulated Models of the Sintering of Metal Powders," *Zeitschrift fur Metallkunde*, 1970, vol. 61, pp. 928-934.

4.   A. J. Markworth and W. Oldfield, "Computer Simulation Studies of Pore Behavior in Solids," *Sintering and Related Phenomena*, G. C. Kuczynski (ed.), Plenum Press, New York, NY, 1973, pp. 209-216.

5.   K. Breitkreutz and D. Amthor, "Monte-Carlo-Simulation des Sinterns durch Volumen-und Oberflachendiffusion," *Metallurgie*, 1975, vol. 29, pp. 990-993.

6.   M. F. Ashby, "A First Report on Sintering Diagrams," *Acta Metallurgica*, 1974, vol. 22, pp. 275-289.

7.   R. M. German and J. F. Lathrop, "Simulation of Spherical Powder Sintering by Surface Diffusion," *Journal of Materials Science*, 1978, vol. 13, pp. 921-929.

8.   P. Bross and H. E. Exner, "Computer Simulation of Sintering Processes," *Acta Metallurgica*, 1979, vol. 27, pp. 1013-1020.

9.   F. B. Swinkels and M. F. Ashby, "A Second Report on Sintering Diagrams," *Acta Metallurgica*, 1981, vol. 29, pp. 259-281.

10.   C. M. Sierra and D. Lee, "Modeling of Shrinkage During Sintering of Injection

Molded Powder Metal Compacts," *Powder Metallurgy International*, 1988, vol. 20, no. 5, pp. 28-33.

11.   K. S. Hwang, R. M. German, and F. V. Lenel, "Analysis of Initial Stage Sintering Through Computer Simulation," *Powder Metallurgy International*, 1991, vol. 23, no. 2, pp. 86-91.

12.   R. M. German, "Overview of Key Directions and Problems in Computational and Numerical Techniques in Powder Metallurgy," *Computational and Numerical Techniques in Powder Metallurgy*, D. S. Madan, I. E. Anderson, W. E. Frazier, P. Kumar, and M. G. McKimpson (eds.), The Minerals, Metals, Materials Society, Warrendale, PA, 1993, pp. 1-15.

13.   H. Riedel, D. Meyer, J. Svoboda, and H. Zipse, "Numerical Simulation of Die Pressing and Sintering - Development of Constitutive Equations," *International Journal of Refractory Metals and Hard Materials*, 1994, vol. 12, pp. 55-60.

14.   K. Y. Sanliturk, I. Aydin, and B. J. Briscoe, "A Finite Element Approach for the Shape Prediction of Ceramic Compacts During Sintering," *Journal of the American Ceramic Society*, 1999, vol. 82, pp. 1748-1756.

15.   R. Raman, T. F. Zahrah, T. J. Weaver, and R. M. German, "Predicting Dimensional Change During Sintering of FC-0208 Parts," *Advances in Powder Metallurgy and Particulate Materials - 1999*, vol. 1, Metal Powder Industries Federation, Princeton, NJ, 1999, pp. 3.115-3.122.

16.   O. Gillia and D. Bouvard, "Phenomenological Analysis and Numerical Simulation of Sintering Application to WC-Co System," *Proceedings of the 2000 Powder Metallurgy World Congress*, Part 1, K. Kosuge and H. Nagai (eds.), Japan Society of Powder and Powder Metallurgy, Kyoto, Japan, 2000, pp. 82-87.

17.   V. Tikare, M. V. Braginsky, E. A. Olevsky, and R. T. Dehoff, "A Combined Statistical-Microstructural Model for Simulation of Sintering," *Sintering Science and Technology*, R. M. German, G. L. Messing, and R. G. Cornwall (eds.), Pennsylvania State University, State College, PA, 2000, pp. 405-409.

18.   A. Zavaliangos and D. Bouvard, "Numerical Simulation of Anisotropy in Sintering Due to Prior Compaction," *International Journal of Powder Metallurgy*, 2000, vol. 36, no. 7, pp. 58-65.

19.   V. Tikare, E. A. Olevsky, and M. V. Braginsky, "Combined Macro-Meso Scale Modeling of Sintering. Part II, Mesoscale Simulations," *Recent Developments in Computer Modeling of Powder Metallurgy Processes*, A. Zavaliangos and A. Laptev (eds.), ISO Press, Ohmsha, Sweden, 2001, pp. 94-104.

20.   R. M. German, *Sintering Theory Practice*, John Wiley & Sons, Inc., New York, NY, 1996.

21.   A. N. Schofield, "Original Cam-Clay," in: *Proceedings of the International*

Conference on Soft Soil Engineering, Guangzhou, November 8–11, 1993.

22. D. C. Drucker and W. Prager, "Soil Mechanics and Plastic Analysis or Limit Design," *Quarterly Appl. Math*, 1952, vol. 10, pp. 157-164.

23. S. Shima and M. Oyane , "Plasticity Theory for Porous Metals," 1976, *Int. J. Mech. Sci* , vol. 18, pp. 285–292.

24. Y.-S. Kwon, S.-H. Chung, K. T. Kim, R. M. German, and H. I. Sanderow, "Numerical Analysis and Optimization of Die Compaction Process," *Advances in Powder Metallurgy and Particulate Materials*, 2003, part. 4, pp. 4-37-4-50.

25. R. M. McMeeking and L. Kuhn, "A Diffusional Creep Law for Powder Compacts," *Acta Metall. Mater.*, 1992, vol. 40, pp. 961-969.

26. T. Kraft and H. Riedel, "Numerical Simulation of Die Compaction and Sintering," *Powder Metallurgy*, 2002, vol. 45, pp. 227-231.

27. P. E. McHugh and H. Riedel, "A Liquid Phase Sintering Model: Application to Si_3N_4 and WC-Co," *Acta Metall. Mater.*, 1997, vol. 45, pp. 2995-3003.

28. D. Bouvard and T. Meister, "Modelling Bulk Viscosity of Powder Aggregate During Sintering," *Modelling Simul. Mater. Sci. Eng.*, 2000, vol. 8, pp. 377-388.

29. A. C. F. Cocks, "The Structure of Constitutive Laws for the Sintering of Fine Grained Materials," *Acta Metallurgica et Materialia*, 1994, vol. 45, pp. 2191-2210.

30. Y. S. Kwon and K. T. Kim, "High Temperature Densification Forming of Alumina Powder—Constitutive Model and Experiments," *Journal of Engineering Materials and Technology*, 1996, vol. 118, pp. 448-455.

31. Y. S. Kwon, Y. Wu, P. Suri, and R. M. German, "Simulation of the Sintering Densification and Shrinkage Behavior of Powder-Injection-Molded 17-4 PH Stainless Steel," *Metallurgical and Materials Transactions A*, 2004, vol. 35, pp. 257-263.

32. R. K. Bordia and G. W. Scherer, "On Constrained Sintering—I. Constitutive Model for a sintering body," *Acta Metallurgica*, 1998, vol. 36, pp. 2393-2397.

33. R. K. Bordia and G. W. Scherer, "On Constrained Sintering—II. Comparison of Constitutive Models," *Acta Metallurgica*, 1998, vol. 36, pp. 2399-2409.

34. R. K. Bordia and G. W. Scherer, "On Constrained Sintering—III. Rigid Inclusions," *Acta Metallurgica*, 1998, vol. 36, pp. 2411-2416.

35. S. H. Chung, Y. S. Kwon, C. M. Hyun, K. T. Kim, M. J. Kim, and R. M. German, "Analysis and Design of a Press and Sinter Process for Fabrication of Precise Tungsten Carbide Cutting Tools," *Advances in Powder Metallurgy and Particulate Materials*, 2004, part. 8, pp. 8-26-8-39.

36. S. J. Park, J. M. Martin, J. F. Guo, J. L. Johnson, and Randall M. German, "Grain Growth Behavior of Tungsten Heavy Alloys Based on Master Sintering Curve Concept," *Metallurgical and Materials Transactions* A, 2006, vol. 37A, pp. 3337-3343.

37. S. J. Park, J. M. Martin, J. F. Guo, J. L. Johnson, and Randall M. German, "Densification Behavior of Tungsten Heavy Alloy Based on Master Sintering Curve Concept," *Metallurgical and Materials Transactions* A, 2006, vol. 37A, pp. 2837-2848.

38. S. H. Chung, Y. S. Kwon, C. Binet, R. Zhang, R. S. Engel, N. J. Salamon, and R. M. German, "Application of Optimization Technique in the Powder Compaction and Sintering Processes," *Advances in Powder Metallurgy and Particulate Materials*, 2002, part. 9, pp. 9-131-9-146.

39. D. Blaine, R. Bollina, S. J. Park, and R. M. German, "Critical Use of Video-imaging to Rationalize Computer Sintering Simulation Models," *Computers in Industry*, 2005, vol. 56, pp. 867-875.

40. S. J. Park, S. H. Chung, J. L. Johnson, and R. M. German, "Finite Element Simulation of Liquid Phase Sintering with Tungsten Heavy Alloys," *Materials Transactions*, 2006, vol. 47, pp. 2745-2752.

41. S. J. Park, R. M. German, P. Suri, D. Blaine, and S. H. Chung, "Master Sintering Curve Construction Software and its Application," *Advances in Powder Metallurgy and Particulate Materials*, 2004, part. 1, pp. 1-13-1-24.

Table 1. The complete set of material properties for die compaction of an iron-based powder [24].

densities	pycnometer density	7.8 g/cm^3
	fractional tap density	0.45
yield function (Shima-Oyane)	α	6.2
	γ	1.03
	m	7.4
flow stress of matrix materials (work hardening)	a	184 MPa
	b	200 MPa
	n	0.24
friction coefficient		0.1
failure surface	d	0.01
	$\tan\beta$	3.41

Table 2. Complete set of material properties for simulating the sintering of W – 8.4 wt.% Ni – 3.6 wt.% Fe [40].

pycnometer density		16.75 g/cm^3	
initial density distribution ρ_0		results from press simulation	
initial mean grain size		0.30 μm	
surface energy γ		2.5 J/m^2	
transition temperature from solid state to liquid phase		1460°C	
friction coefficient		0.3	
sintering stress	$\sigma_s = \dfrac{6\gamma}{G}\dfrac{\rho^2(2\rho-\rho_0)}{\theta_0}$ for $\rho < 0.85$ $\sigma_s = \dfrac{2\gamma}{G}\left(\dfrac{6\rho}{\theta}\right)^{1/3}$ for $\rho_W > 0.95$ $\sigma_s = \dfrac{(\rho_2-\rho)}{(\rho_2-\rho_1)}\sigma_{si} + \dfrac{(\rho-\rho_1)}{(\rho_2-\rho_1)}\sigma_{sf}$ for $0.85 \leq \rho_W \leq 0.95$			
state			solid	liquid
grain growth	$\dfrac{dG}{dt} = \dfrac{k_0 \exp(-Q_G/RT)}{G^l}$	k_0 (m^{n+1}/s)	2.8·10^{-13}	1.1·10^{-15}
		Q_G (kJ/mol)	241	105
		l	2.0	2.0
bulk viscosity	$K_i = \dfrac{\rho(\rho-\rho_0)^2}{8\theta_0^2}\dfrac{TG^3}{\alpha_i \exp(-Q_D/RT)}$ for $\rho \leq 0.92$ $K_f = \dfrac{\rho}{8\theta_0^{1/2}}\dfrac{TG^3}{\alpha_f \exp(-Q_D/RT)}$ for $\rho > 0.92$ with $\alpha_f = \dfrac{\theta_0^2}{\sqrt{0.08}(0.92-\rho_0)^2}\alpha_i$	Q_D (kJ/mol)	250	250
		α_i (m^6·K/s)	1.3·10^{-17}	5.0·10^{-17}
shear viscosity	$\mu_i = \dfrac{\rho^2(\rho-\rho_0)}{8\theta_0}\dfrac{TG^3}{\beta_i \exp(-Q_D/RT)}$ for $\rho \leq 0.92$ $K_f = \dfrac{\rho}{8}\dfrac{TG^3}{\beta_f \exp(-Q_D/RT)}$ for $\rho > 0.92$ with $\beta_f = \dfrac{\theta_0}{0.92(0.92-\rho_0)}\beta_i$	β_i (m^6·K/s)	1.3·10^{-17}	1.3·10^{-12}

Note than R is the universal gas constant, ρ is the density, $\theta (= 1 - \rho)$ is the porosity, $\theta_0 (= 1 - \rho_0)$ is the initial porosity, and ρ_w is the density of tungsten skeleton.
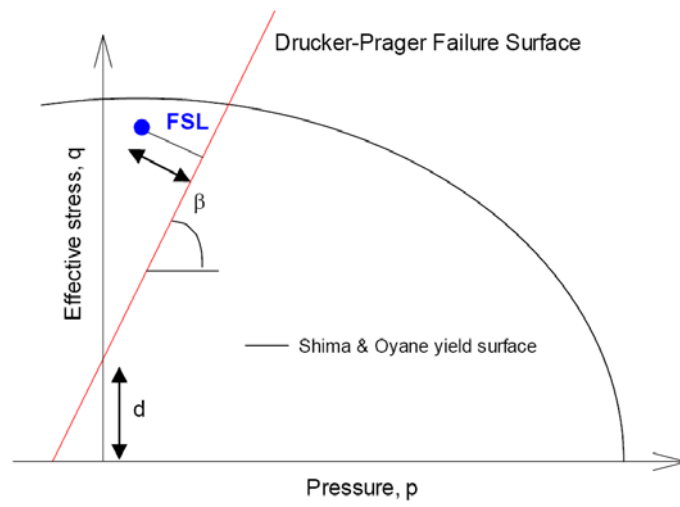
Figure 1. Definition of failure separation length (FSL) based on Shima and Oyane yield model and Drucker-Prager failure surface.
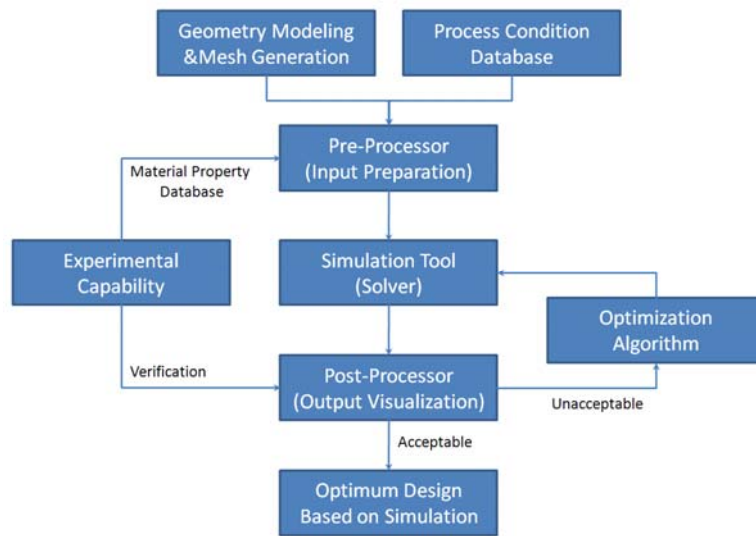
Figure 2. Typical procedure for computer simulation for press and sinter process.

(a) meshed compact	(b) modeling for compaction	(c) modeling for sintering
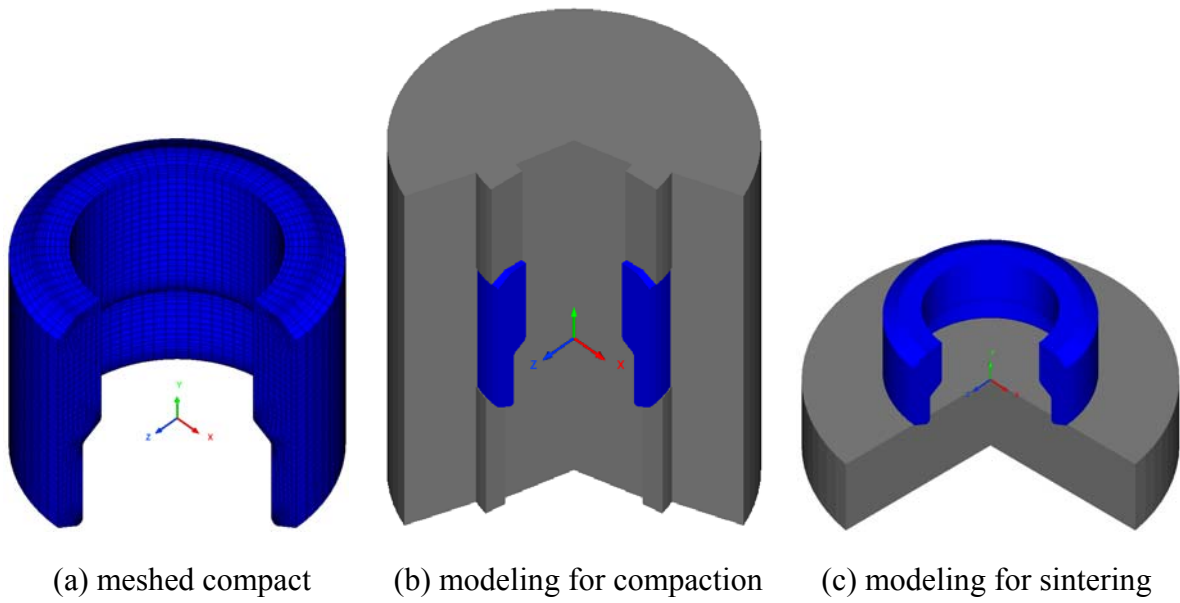
Figure 3. Example modeling and mesh generation example showing the simulation of compaction and sintering for an oxygen sensor housing; (a) mesh generation for the compact, (b) modeling of punches and dies during compaction for the press simulation, and (c) modeling of compact in contact with the substrate during sintering simulation.
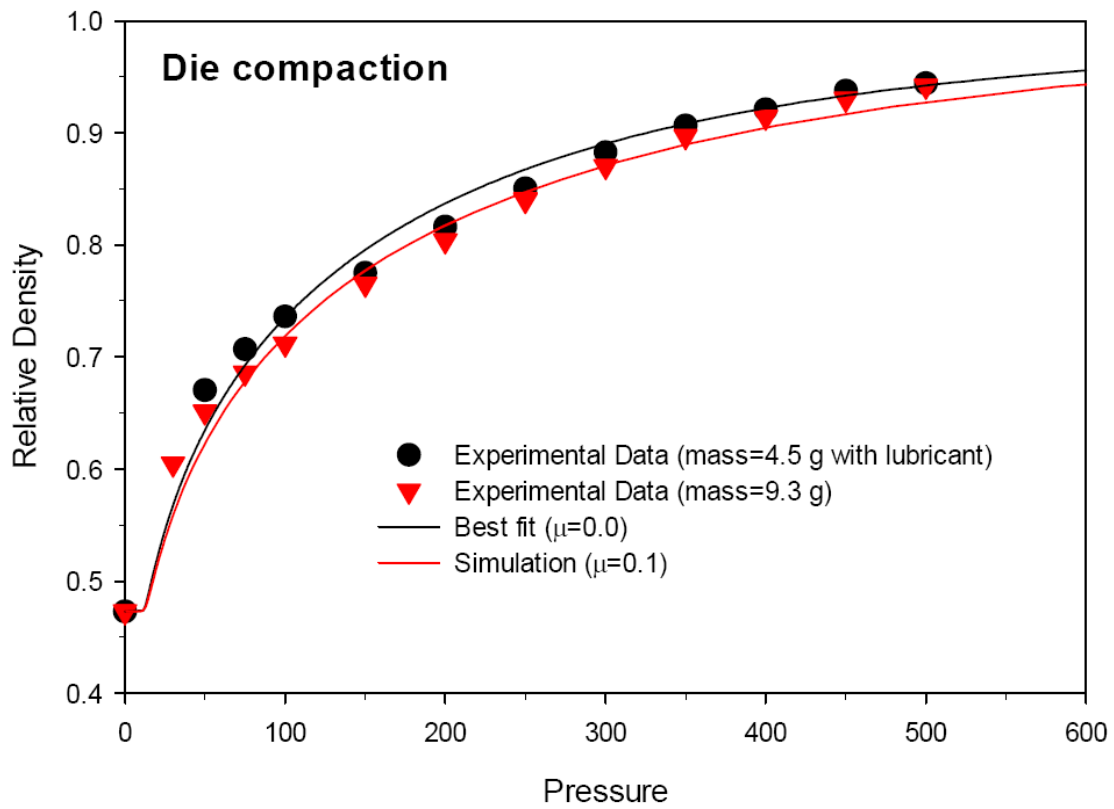
Figure 4. An example compaction curve for a iron-based powder, showing the relative density model results versus compaction pressure in MPa with no friction and with a friction coefficient of 0.1 for two compact samples [24].
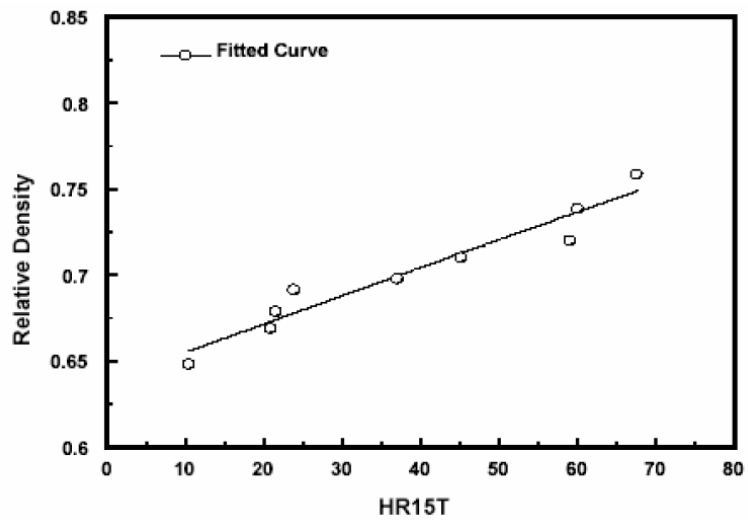
Figure 5. Plot of relative density and Rockwell 15T scale hardness for the die compaction of a WC-Co powder [35].
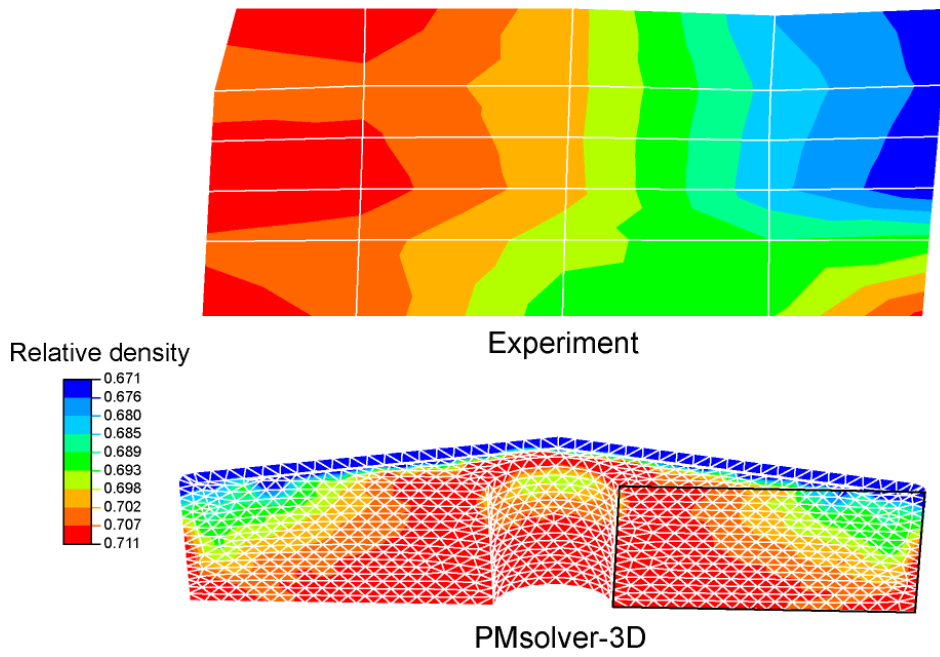
Figure 6. Comparison between the computer simulated green density gradients (PMsolver) and the experiment results taken from hardness tests on a cross-sectioned green compact of a cutting tool formed from WC-Co powder [35].
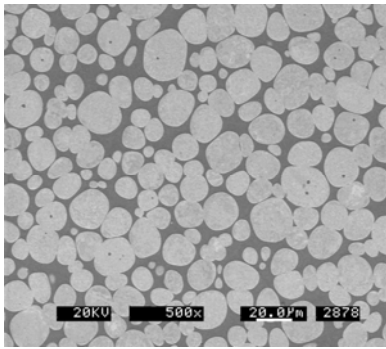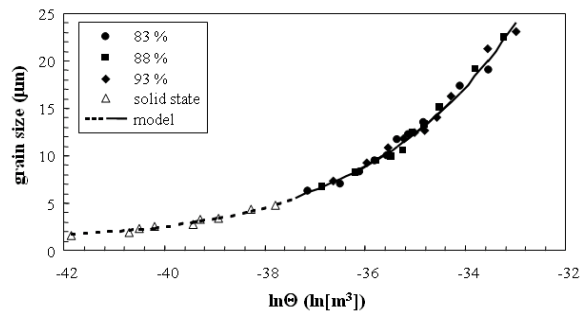
| (a) SEM micrographs | (b) grain growth modeling |

Figure 7. (a) A scanning electron micrograph of a liquid phase sintered tungsten heavy alloy (W – 8.4 wt.% Ni – 3.6 wt.% Fe) after quenching and (b) the grain size model results taken from an integral work of sintering concept that includes only the thermal cycle (time-temperature path) to predict grain size for any point in a heating path for three different tungsten contents [36].
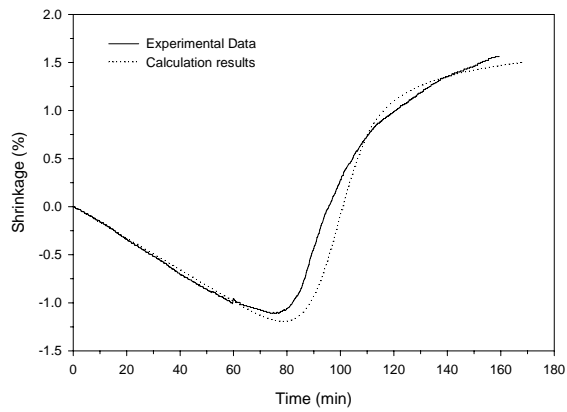
(a) shrinkage with time   (b) shrinkage with temperature
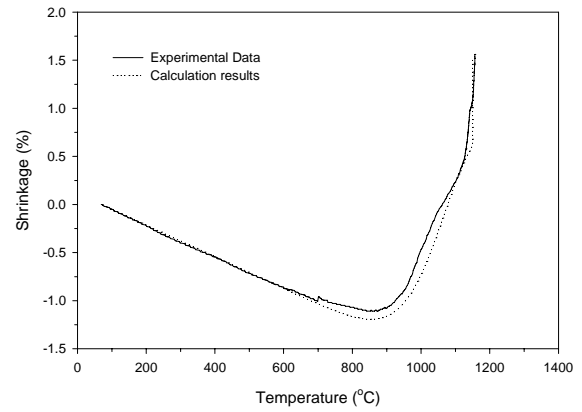
Figure 8. Dilatometry data showing *in situ* shrinkage data during constant heating rate experiments and the curve-fitting results used to obtain the material parameters to predict densification of a 316L stainless steel powder [38].
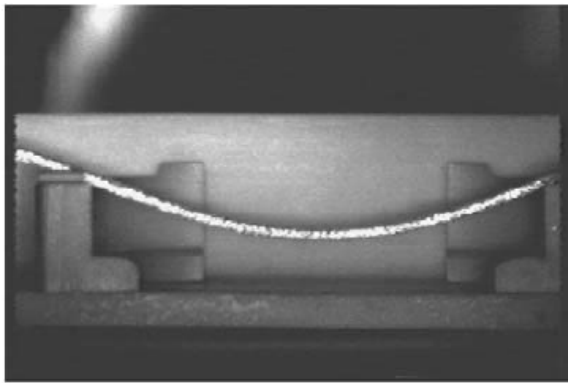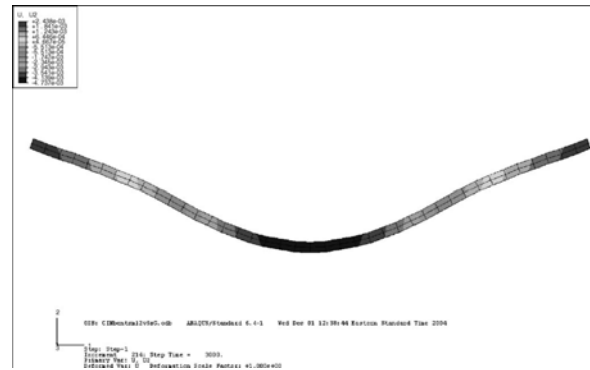
(a) in situ bending test	(b) FEM simulation

Figure 9. (a) A video image taken during the *In situ* bending test for a 316L stainless steel sample doped with 0.2 wt. % boron, and (b) the FEM model results used to verify the shear viscosity property as a function of time, temperature, grain size, and density during heating [39].
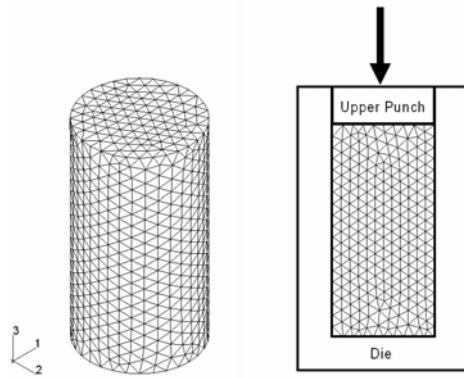
(a) meshed geometry
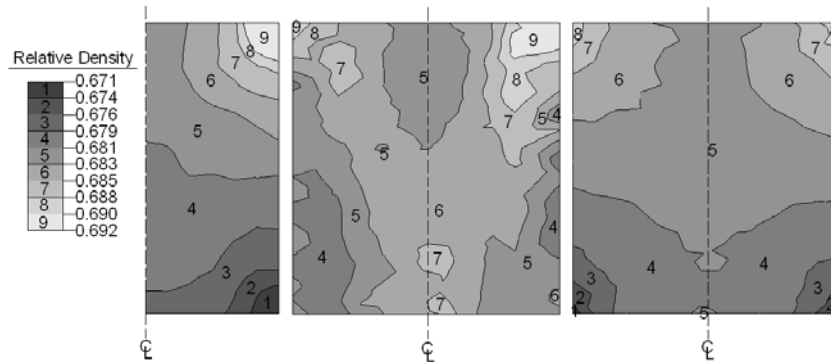
(b) result from experiment, explicit method, and implicit method

Figure 10. Comparison of explicit and implicit methods for compaction simulation in the WC-Co system, where the half-axis experimental result is given on the left and the full-axis explicit method result is shown in the center and the implicit method result is on the right [35].
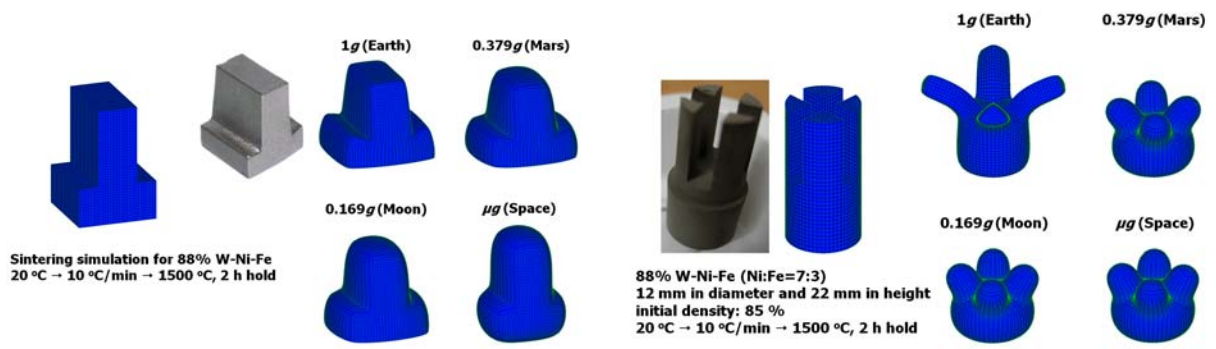
(a) T-shape   (b) joint part

Figure 11. Final distorted shape by sintering under various gravitational environments for complicated test geometries [40].
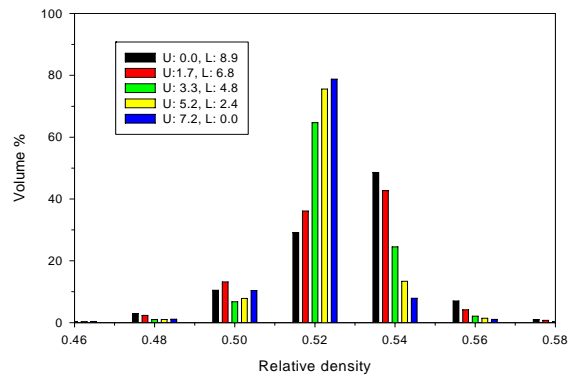
(a) histogram for different processing conditions
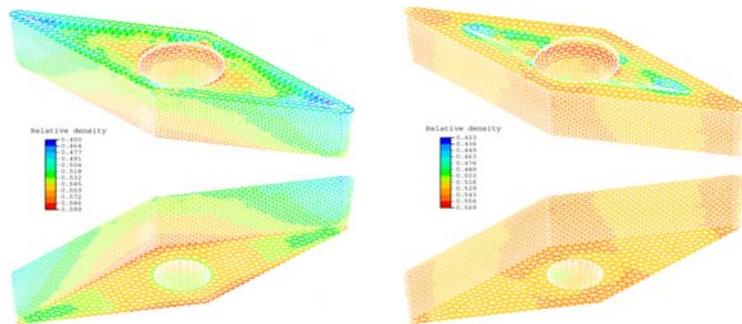
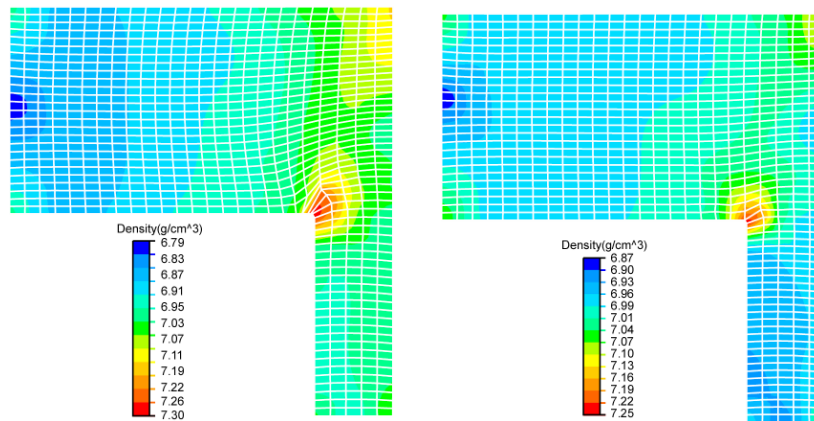(b) green density distributions in the initial and optimum designs

Figure 12. Optimization for uniform density distribution during die compaction for a cutting tool fabricated from WC-Co [35].
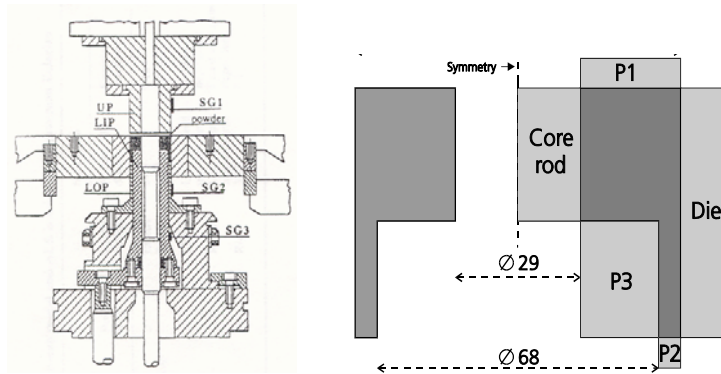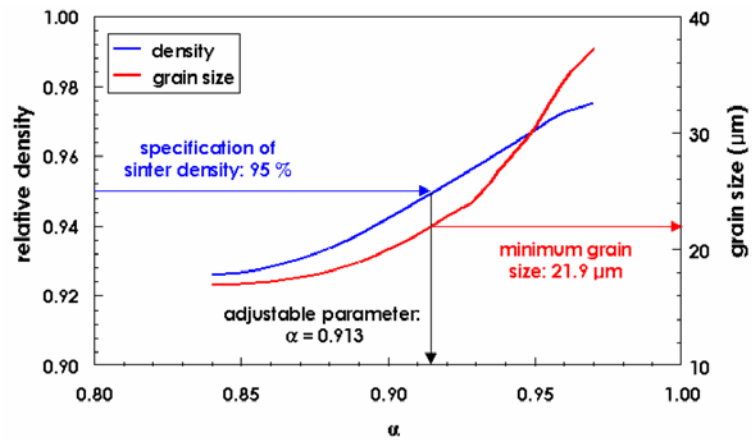
(a) compaction tool set and analysis domain
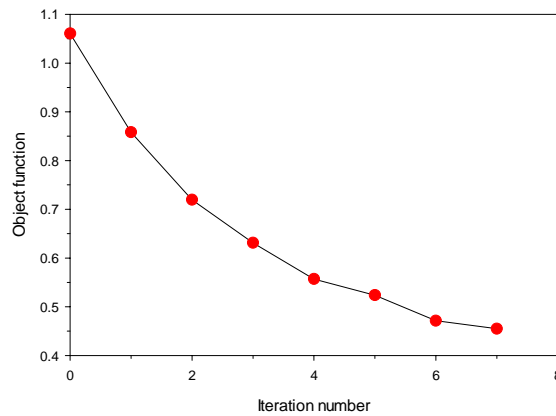
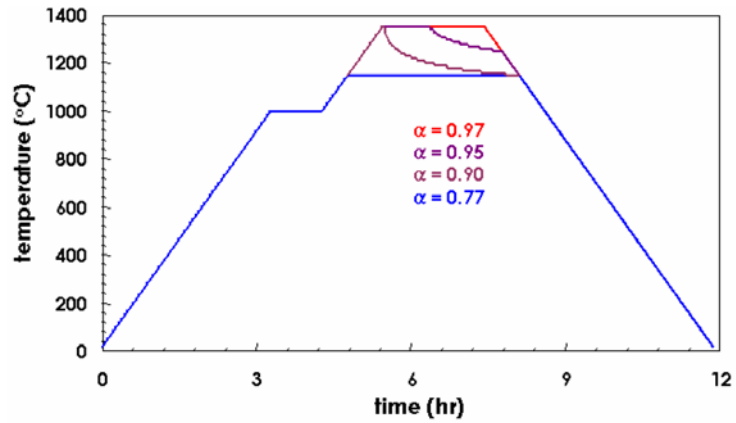(b) variation of objective function during optimization iteration

(c) green density distributions in the initial and optimum designs

Figure 13. Optimization to minimize the green density gradients during die compaction of a steel hub component [24].
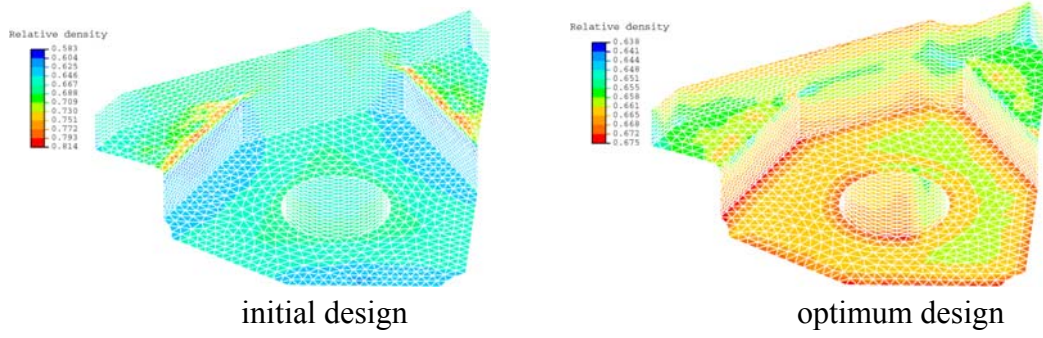
(a) sintered density and the corresponding minimum grain size


(b) corresponding sintering cycle

Figure 14. Minimum grain size for a given final sinter density and the corresponding sintering cycle for achieving this goal in a 17-4 PH stainless steel [41].

initial design   optimum design

(a) simulation result of green density gradients

initial design   optimum design

(b) experimental result of green compact

initial design   optimum design
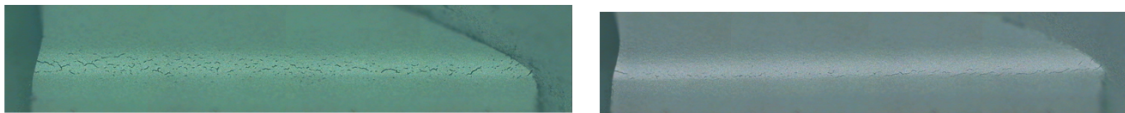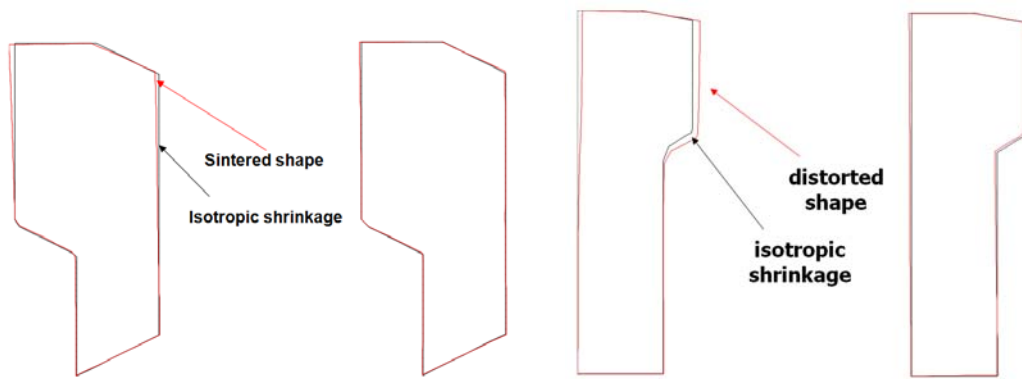
(c) experimental result of sintered compact

Figure 15. The effect of density distribution after die compaction on sintering and the formation of corner cracks.

(a) initial and optimum holder designs   (b) initial and optimum sleeve designs

Figure 16. Final part profile files based on the combined press-sinter simulation for the optimized design of a holder and sleeve for an oxygen sensor.